Title
Frequent rainfall-induced new particle formation within the canopy in the Amazon rainforest

Journal
Nature Geoscience, 17(12)

ISSN
1752-0894

Authors
Machado, Luiz AT
Unfer, Gabriela R
Brill, Sebastian
et al.

Publication Date
2024-12-01

DOI
10.1038/s41561-024-01585-0

nature geoscience

Article

https://doi.org/10.1038/s41561-024-01585-0

Frequent rainfall-induced new particle formation within the canopy in the Amazon rainforest

Received: 9 July 2024

Accepted: 15 October 2024

Published online: 8 November 2024

Check for updates

A list of authors and their affiliations appears at the end of the paper

Atmospheric aerosol particles are essential for forming clouds and precipitation, thereby influencing Earth's energy budget, water cycle and climate on regional and global scales. However, the origin of aerosol particles over the Amazon rainforest during the wet season is poorly understood. Earlier studies showed new particle formation in the outflow of deep convective clouds and suggested a downward flux of aerosol particles during precipitation events. Here we use comprehensive aerosol, trace gas and meteorological data from the Amazon Tall Tower Observatory to show that rainfall regularly induces bursts of nanoparticles in the nucleation size range. This can be attributed to rain-related scavenging of larger particles and a corresponding reduction of the condensation sink, along with an ozone injection into the forest canopy, which could increase the oxidation of biogenic volatile organic compounds, especially terpenes, and enhance new particle formation. During and after rainfall, the nucleation particle concentrations directly above the canopy are greater than those higher up. This gradient persists throughout the wet season for the nucleation size range, indicating continuous particle formation within the canopy, a net upward flux of newly formed particles and a paradigm shift in understanding aerosol–cloud–precipitation interactions in the Amazon. Particle bursts provide a plausible explanation for the formation of cloud condensation nuclei, leading to the local formation of green-ocean clouds and precipitation. Our findings suggest that an interplay of a rain-related reduction in the condensation sink, primary emissions of gases, mainly terpenes, and particles from the forest canopy, and convective cloud processing determines the population of cloud condensation nuclei in pristine rainforest air.

Cloud droplet formation and growth depend on the abundance and properties of atmospheric aerosol particles serving as cloud condensation nuclei (CCN)[1–3]. Primary particles are directly emitted from natural or anthropogenic sources, and secondary particles can be generated in the atmosphere through new particle formation (NPF)[4]. While the radiative forcing of trace gases is well known, the influence of aerosol particles on clouds and radiation is much more uncertain[5]. The transformation of gases into particles[6] is critical for the radiative budget, hydrological cycle, climate, air quality and public health. Condensable vapours can form particles that scatter or absorb radiation and initiate cloud formation when they become large enough to serve as CCN[7,8].

Atmospheric NPF involves the oxidation of volatile compounds to generate condensable vapours that can form stable molecular clusters through nucleation and undergo further growth by condensation or coagulation[4,6]. Chamber experiments have shown that the oxidation of biogenic volatile organic compounds (BVOC), such as terpenes, can

e-mail: l.machado@mpic.de

generate organic vapours of extremely low volatility, initiate NPF and produce secondary organic aerosol in the absence of sulfuric acid, a common precursor of NPF[9–11]. A recent field study in the transition region between temperate and boreal forests in Canada confirmed that NPF can occur without sulfuric acid precursor sources and suggested nucleation of extremely low-volatility organics as a source[12]. Under pristine conditions in the Amazonian wet season, sulfate concentrations are also very low, and the origin of the background aerosol population has remained enigmatic for decades (for example, refs. 13–15).

NPF events in which the size distribution evolves in a characteristic 'banana' shape starting around 10 nm or even lower are rarely observed in the Amazon region[16], but rain-induced particle bursts occur frequently during the wet season[17]. Ground-based measurements at the Amazon Tall Tower Observatory (ATTO) revealed that 28% of the days between January and June, which are the rainiest months, were characterized by a sudden occurrence of particles with diameters smaller than 50 nm (ref. 18). In the course of rainfall events, particles in the nucleation mode size range (<50 nm) can increase in concentration, whereas levels of large Aitken particles and accumulation mode particles tend to decrease[19] due to CCN activation and precipitation scavenging[20,21]. Rainfall further decreases the condensation sink and, accordingly, the rate at which vapours condense onto existing particles, thereby facilitating new particle formation.

Observational studies and large eddy simulations have demonstrated that deep convective clouds can efficiently transport BVOC and other reactive trace gases and promote NPF in the upper troposphere[22–25]. The appearance of new particles in the Amazonian boundary layer has been attributed to downdraft events that bring down particles from the upper troposphere, which is rich in freshly nucleated particles[23,25–27]. However, downdrafts occur mainly in the low to middle troposphere[19], and NPF in the upper troposphere occurs in the outflow of deep convective systems, that is, outside the boundaries and internal downdrafts of clouds[28]. Studies based on large eddy simulations[29] have revealed that the primary source of particles in downdrafts is the middle troposphere at approximately 5 km altitude and that particles originating from the upper troposphere cannot reach the surface within a 2 hour time frame. Global model simulations incorporating a regional nested high spatial resolution model[30] demonstrated that vertical transport of freshly nucleated particles in the upper troposphere is not expected to contribute to boundary-layer aerosol concentrations within the timescale of a few days.

Climate change and deforestation are rapidly changing the environmental balance of the Amazon[31,32]. Unravelling fundamental processes in Amazonian atmosphere–biosphere exchange, such as the spatiotemporal patterns and importance of NPF as a potential source of the natural background aerosol, is thus of particular importance because the wet season in the central Amazon rainforest allows the study of the interaction and evolution of aerosols, clouds and precipitation under near-pristine and preindustrial-like conditions. In addition, atmospheric circulation patterns are altered on synoptic scales, for example, through a changing El Niño/La Niña frequency, affecting long-range transport, downdraft characteristics, rainfall patterns and, consequently, Earth's radiative budget. Our ability to forecast these changes in Amazonia and beyond will depend largely on a correct representation of fundamental processes, including aerosol–cloud interactions in regional and global climate and Earth system models.

In this Article, we combine multiple long-term measurement datasets from ATTO[32] at different altitudes inside and above the rainforest canopy (0.05–325 m above ground). Moreover, we use data from the recently established ATTO Campina site, which is equipped with a broad spectrum of remote-sensing techniques. The combination of measurements and modelling of the vertical atmospheric profile and dynamics, as well as boundary-layer concentrations of aerosols and reactive and nonreactive trace gases, provide unique insights into the atmospheric processing of the Amazonian biogeochemical reactor.

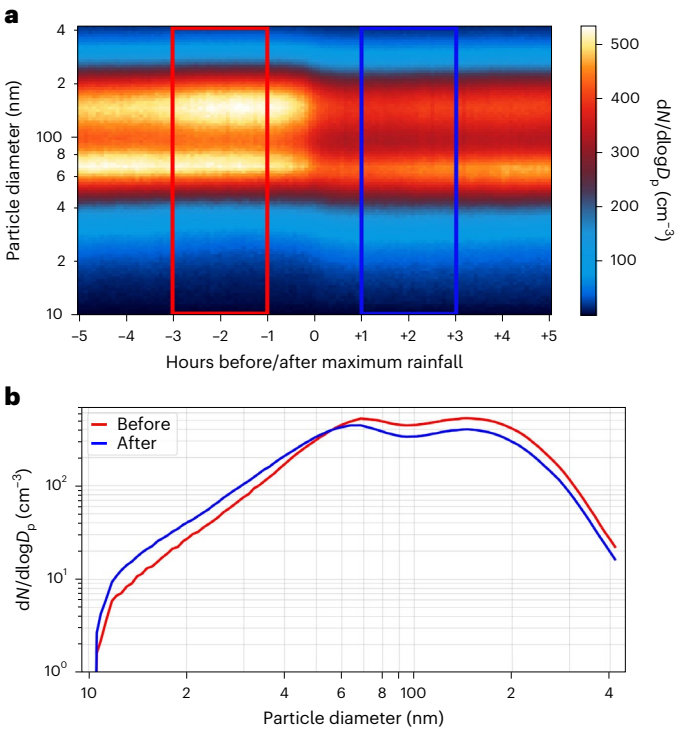

Fig. 1 | Aerosol particle number–size distribution, before and after precipitation. a, Evolution of aerosol particle number–size distributions at an altitude of 60 m from 5 hours before to 5 hours after the maximum rainfall intensity. Shown is a composite of 391 rain events between February and May from 2018 to 2020. dN/dlogD_p denotes the particle distribution. **b**, Median size distribution for particles in the time ranges of −3 to −1 hour before and +1 to +3 hours after the maximum rain intensity. Details on the SMPS measurements and data processing can be found in Methods ('SMPS and data processing' and 'Composites and data processing' sections). The data were averaged over 391 rain events with rain rates > 0.5 mm h^{-1}.

We explore largely unresolved processes in the complex cascades of atmospheric chemistry–meteorology and aerosol–cloud interactions and feedback loops, which are characteristic of the Amazon 'Green Ocean' atmosphere. Our focal point is the interplay of rainfall, aerosols and new particle formation during rain events.

Interplay of rainfall, aerosols and NPF

During rain events, there is a marked increase in the concentration of particles in the sub-40 nm range, highlighting a direct link between aerosol particle bursts and precipitation. Figure 1a illustrates the temporal evolution of aerosol particle number–size distributions observed above the rainforest canopy (60 m) during the wet season. The contour plot, which extends from 5 hours before to 5 hours after the maximum rainfall intensity, shows a marked decrease in the concentration of particles in the upper size range (accumulation and Aitken modes), concurrently with an increase in the concentration of particles in the size range below 40 nm (small particles from the Aitken mode and the nucleation mode). Figure 1b shows the average size distributions before (−3 to −1 hour) and after (+1 to +3 hour) the maximum rain rate. Decreased particle concentrations in the accumulation and Aitken modes after rainfall and, by contrast, increased sub-40 nm mode concentrations after the rainfall event are evident.

To investigate the processes related to NPF and rainfall, we analysed the temporal evolution of ultrafine particle number concentrations in five size classes with diameters from 10 to 100 nm, near the canopy at 60 m and at the top of the tall tower at 325 m. The lowest two size classes of 10–20 nm and 20–40 nm are characteristic for the nucleation mode of atmospheric aerosols, that is, newly formed

https://doi.org/10.1038/s41561-024-01585-0

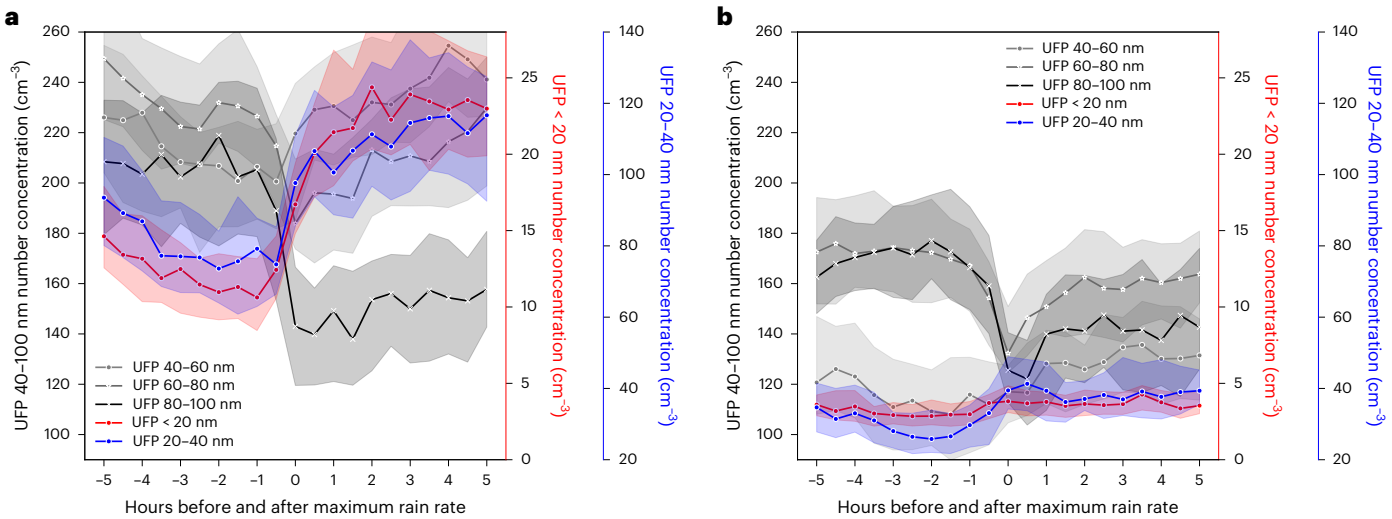

Fig. 2 | Aerosol particle number–size distribution during rain events close to the canopy and above. Median particle concentrations in different size ranges between February and May for 2018–2020, showing 5 hours before to 5 hours after the maximum rainfall event. **a**, 60 m elevation. **b**, 325 m elevation. Particle concentrations are divided into the following classes: 10–20 nm (blue), 20–40 nm (red) and the classes 40–60 nm, 60–80 nm and 80–100 nm (grey tones). For 60 m, the increase in the concentration of particles smaller than 40 nm was observed 0.5 hour before the maximum rainfall event up to 1.0 hour later. Larger particles decreased in concentration following rainfall. At 325 m, the increase in nucleation particles was not well defined. Colour-shaded bands represent 95% confidence intervals. The composite was made over 391 rain events with rain rates > 0.5 mm h^{-1}. UFP, ultrafine particles.

particles that have undergone rapid initial growth by coagulation and condensation since they were freshly nucleated from molecular clusters with critical sizes around 3 nm (ref. 33). The measurements performed immediately above the forest canopy (60 m above ground) reveal (Fig. 2a) an increase in particle number concentration in the nucleation size range, which is a clear indication for NPF[4], from about 1 hour before to 1 hour after maximum rainfall intensity. By contrast, the concentration of large Aitken and accumulation mode particles exhibits a strong decrease as expected due to CCN activation and precipitation scavenging. The measurements performed higher above the forest canopy (325 m above ground) exhibit similar patterns for Aitken and accumulation mode particles but at substantially lower concentration levels (Fig. 2b). The concentration decrease is even stronger for particles in the nucleation size range, and the increase after maximum rainfall intensity is much less pronounced. The data have been corrected for particle losses in the sample inlet to exclude systematic bias between the measurements at different altitudes. In addition, an elevator was installed at the ATTO tower, continuously profiling between 8 and 318 m, confirming the results (see Methods for scanning mobility particle sizer (SMPS) data ('SMPS and data processing' section) and for the composite methodology ('Composites and data processing' section) and Supplementary Fig. 1). The different concentration levels observed at 325 m and 60 m altitude suggest that the source of the new particles is in the forest near or within the canopy during rain events in the wet season over the Amazon.

The decrease in particles larger than 40 nm due to precipitation leads to a decrease in the condensation sink, thus promoting the formation of nucleation particles. Figure 3 presents a comprehensive analysis of the condensation sink (see Methods (Condensation sink) for details on the calculation), covering the 5 hours before and after the peak rainfall intensity. The condensation sink exhibits an increasing trend up to 1 hour before maximum rainfall, followed by a sharp decline from 1.3 to 0.9 × 10^{-3} s^{-1} within the +0.5 hour window and a gradual but continuous increase later. The temporal reduction in maximum precipitation aligns with an increase in the concentration of nucleation particles, suggesting a fundamental role in the process of NPF. Notably, after 0.5 hour, the condensation sink gradually increases while the nucleation particles continue to rise modestly, indicating

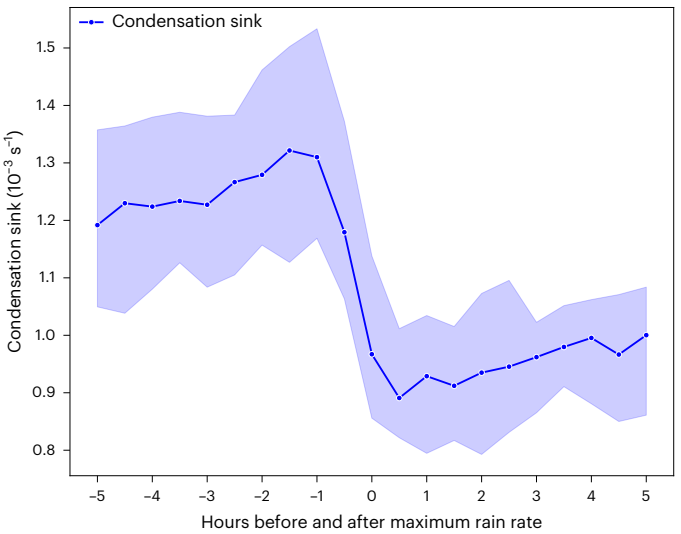

Fig. 3 | The evolution of condensation sink during rain events. Median concentration of the condensation sink for ATTO between February and May for 2018–2020, computed from the SMPS data at 60 m from 5 hours before to 5 hours after the maximum rainfall event. The condensation sink increases before the rain until 1 hour before the maximum rainfall, followed by a drastic reduction from 1.3 to 0.9 × 10^{-3} s^{-1} until +0.5 hours and then a continuous slight increase. Colour-shaded bands represent 95% confidence intervals. The composite was made over 391 rain events with rain rates > 0.5 mm h^{-1}.

the involvement of distinct mechanisms in producing new particles. A box model was used to evaluate the formation of new particles from the surface up to 79 m, confirming the clustering process and subsequent atmospheric nucleation and the effect of reducing the condensation sink (see Methods (Box model) and Supplementary Fig. 2).

New particles are observed forming close to the canopy

An important feature of rainfall events is the injection of O_3 from the relatively ozone-rich free troposphere into the boundary layer[26,34,35].

https://doi.org/10.1038/s41561-024-01585-0

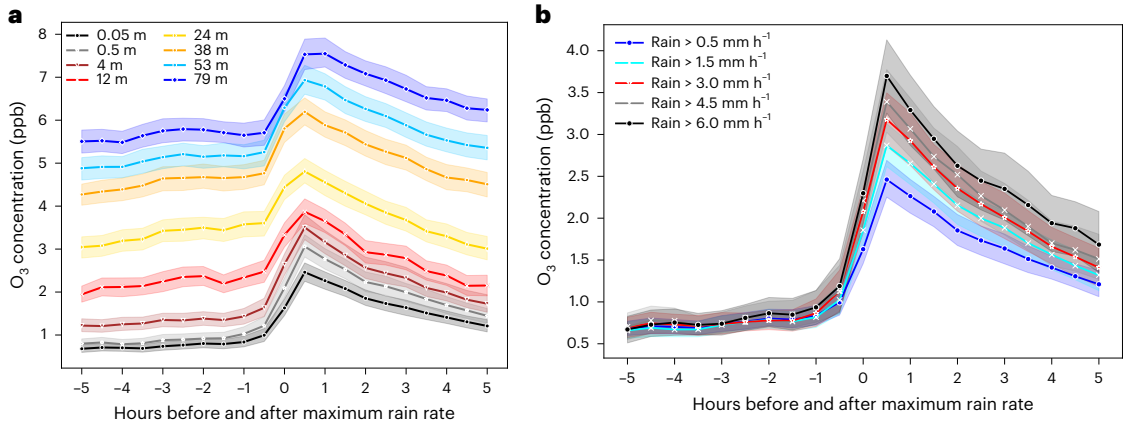

Fig. 4 | Ozone evolution before and after precipitation as a function of the height and rain rate. The O_3 concentration profiles between 0.05 and 79 m, averaged over the wet-season months (February to May) from 2018 to 2020. Representation here is synchronized to rainfall events, covering 5 hours before and 5 hours after maximum rainfall. **a**, The entire profile. **b**, The 0.5 m altitude, classified by different rainfall intensities. Colour-shaded bands represent 95% confidence intervals. The composite was made over 336 rain events with rain rates > 0.5 mm h^{-1}. The O_3 concentration increases up to three times relative to the pre-rain conditions and peaks about 1 hour after the rainfall maximum. The offset between the peaks in rainfall and O_3 concentration does not depend on rainfall intensity, while the increase in O_3 concentration depends on rainfall intensity.

Figure 4a shows the temporal evolution of the O_3 concentration at different heights (from 0.05 to 79 m) 5 hours before to 5 hours after maximum rainfall intensity. The O_3 concentration inside the forest canopy can increase by more than a factor of three. The O_3 enhancement is modulated by rainfall intensity, but with a phase lag (time interval) of approximately half an hour between the maximum rainfall and maximum O_3 concentration (Fig. 4b). A clear relationship exists between the ozone injected by the rainfall event and the NPF. The Amazon forest also releases large amounts of BVOC, including isoprene, monoterpenes and sesquiterpenes emitted by vegetation and soil[36,37]. Mosses and lichen, which constitute a significant portion of the forest ground cover, release sesquiterpenes when they become moist.

Figure 5 shows the temporal evolution of O_3, NO, NO_2, isoprene, monoterpenes (see Methods (O_2, NO and NO_2 data processing periods and Isoprene and monoterpene data processing periods) for data description) and particles in the nucleation size range sub-40 nm during rainfall events. The O_3 increases while isoprene and monoterpenes decrease sharply. The concentrations of NO_2 and nucleation mode particles increase less steeply and reach a maximum approximately 1 hour after maximum rainfall intensity. During the following hours, the concentrations of O_3 and NO_2 decrease again, while the concentration of nucleation mode particles remains nearly constant. Monoterpene concentrations reach the minimum when sub-40 nm particles reach the highest concentration. The rapid decline in BVOC concentrations at 80 m can be explained by dilution caused by the downdraft, lower emissions due to reduced solar radiation and temperature, but also by increasing chemical loss through oxidation and the formation of highly oxygenated organic molecules (HOMs) and low-volatility organic compounds (LVOCs). Observations show that the concentration near the ground normally increases with rain[38,39] or in chamber experiments[40]; the same behaviour was observed with sesquiterpenes[41]. At maximum precipitation, the wind speed increased by more than 50%, and solar radiation intensity diminished (Supplementary Fig. 3). The decrease in air temperature by approximately 10% and the corresponding increase in relative humidity occur at a slower pace, reaching their maximum extent 0.5 to 1.0 hour after the maximum precipitation event (see Methods (Weather data processing and periods) for data description). The NO_2, which is in the opposite phase to NO, shows a slower increase compared with the rapid increase of O_3. The high concentration of O_3 favours the fast chemical conversion of NO into NO_2. At the same time, rain continues to bring down ozone-rich air during the process. Size-resolved chemical analysis of aerosol particles

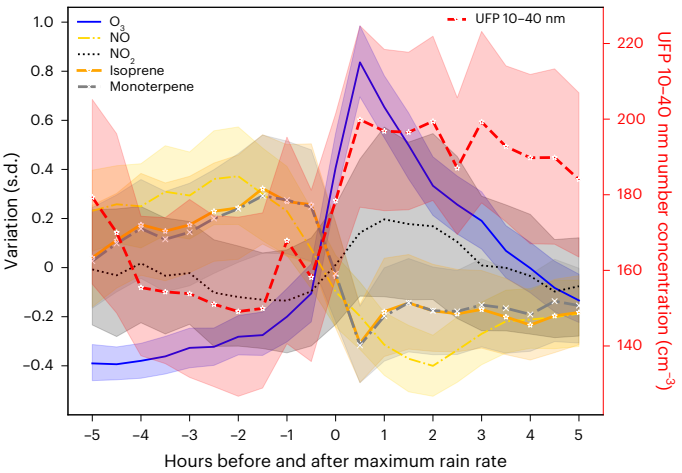

Fig. 5 | Gas and aerosol evolution before and after precipitation. Composite plot of ATTO trace gas and aerosol data during rain events, using a normalized representation, which shows data from 5 hours before to 5 hours after the rainfall peak for the 2018–2020 wet seasons (February to May). The left axis shows the variation of NO_2 at 12 m height, NO at 0.5 m, O_3 at 4 m, isoprene at 80 m and monoterpenes at 80 m in units of standard deviations. The right axis shows the variation of nucleation particles (10–40 nm) at 60 m in absolute number concentration. The rain-related concentration changes show increases in O_3 and NO_2, decreases in NO, isoprene and monoterpenes, and an increase in nucleation particles. All time series incorporate wet-season data (that is, February to May) from 2018 to 2020. Colour-shaded bands represent 95% confidence intervals. The composite was made over 391 rain events with rain rates > 0.5 mm h^{-1}. For NO, NO_2 and O_3, 114, 94 and 336 rain events, respectively, were used, and for isoprene and monoterpene, 90 rain events were used for the composite.

conducted at the ATTO research site offers a compelling demonstration of the rapid formation of fresh particles resulting from swift chemical reactions occurring directly above the forest canopy (see Methods (Micro-orifice uniform deposition impactors data and experiment) and Supplementary Fig. 4).

The nucleation mode particles show a slow increase, indicating that they are not brought down with the descending air current but rather are newly formed due to the reduction of the condensation sink and the chemical reactions that form secondary organic aerosol precursors. Concentrations of particles below 40 nm persist at elevated

https://doi.org/10.1038/s41561-024-01585-0

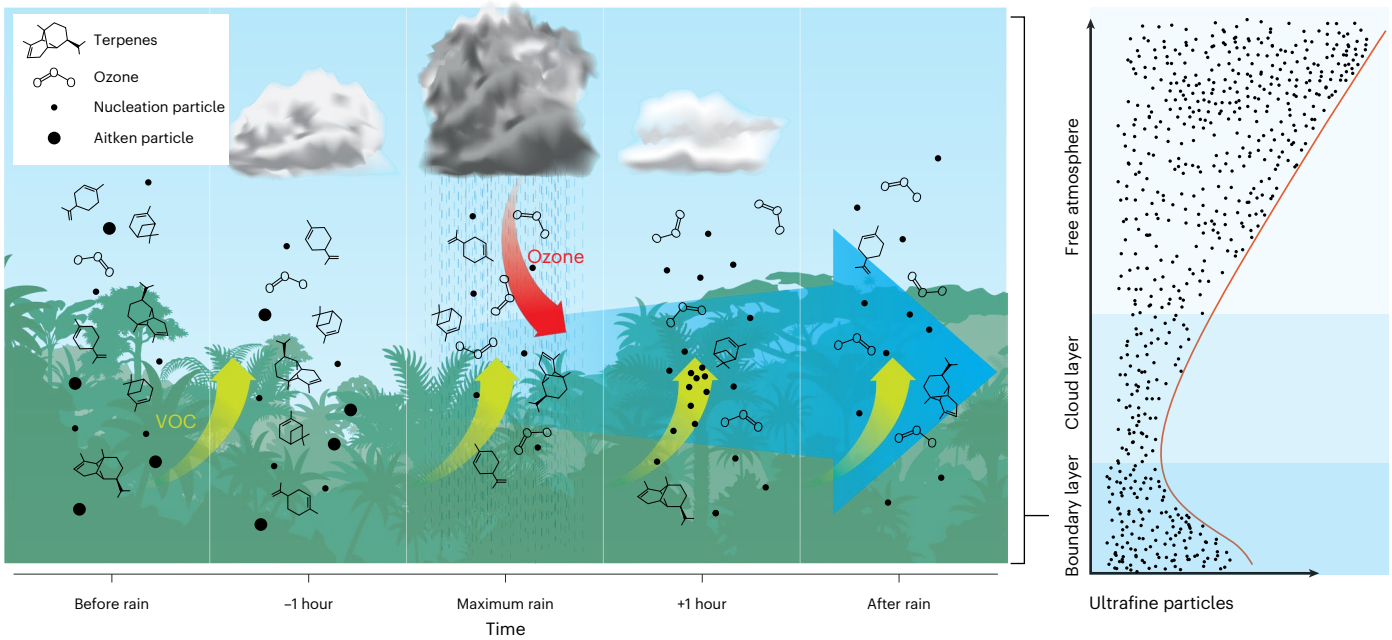

Fig. 6 | The gas–aerosol processes occurring during rainfall events. Concentrations of ozone, BVOC (monoterpenes–sesquiterpenes) and particles before and after the maximum rain rate, during the night and the early morning of the following day.

levels for up to 5 hours following a rain event. This phenomenon is probably linked to the release of sesquiterpenes after rain, as distinct sesquiterpene species continue to be emitted for up to 6 hours after heavy rainfall, in contrast to subsequent dry days[41]. Another contributing factor is the rainfall timing, which typically occurs in the late afternoon and evening. Ultrafine particles become trapped within the nocturnal boundary layer, with their concentrations remaining relatively stable throughout the night. Subsequently, there is a significant decrease in the morning, accompanied by an increase in the Aitken and accumulation modes[19]. All these processes highlight the importance of considering local processes in understanding particle dynamics during precipitation events.

A characteristic feature of NPF is the growth of newly formed particles from the nucleation to the Aitken size range. To investigate this process, we analysed the diurnal evolution of the aerosol particle size distribution for days with different O_3 concentration levels at night, as shown in Supplementary Fig. 5. Days with high nighttime O_3 levels are days with rainfall occurring during the late afternoon and nighttime. The physical mechanism responsible for higher nighttime O_3 concentrations was the late-afternoon and nighttime convection that injects O_3 into the canopy. High O_3 nighttime concentrations are associated with rainy nights; by contrast, low nighttime O_3 concentrations are associated with the absence of rain events during the night. The convective boundary layer begins to decay at sunset, giving rise to the nocturnal boundary layer[42]. During the wet season, the nocturnal boundary layer is lower than 400 m, and the air within the canopy becomes isolated from the free atmosphere. If a particle burst occurs in the evening or at night, the concentration of sub-40 nm particles remains nearly unchanged due to their relatively long lifetime of several hours[43]. The O_3 injected during nighttime rainfall events remains trapped inside the canopy and can lead to high nighttime O_3 concentrations despite the continuous production of NO from the soil that consumes O_3 throughout the night. When sunlight reaches the canopy, growth process events can be easily identified on days with higher previous nighttime O_3 concentrations. Measurements of the oxygenated and total organic aerosol concentrations at 60 and 325 m by two aerosol chemical speciation monitors (ACSMs) shed more light on the early morning growth process (see data description and methodology in Methods (ACSM data periods) and Supplementary Fig. 6).

Intrinsic link between nucleation, gases and precipitation

In this Article, we propose an intrinsic relationship between sub-40 nm particles, reactive trace gases and weather events in the Amazon. Rainfall events change the trace gas concentrations considerably just above the canopy and produce bursts of sub-40 nm particles, which grow into the Aitken mode size range during the early morning of the next day. Our findings highlight several aspects of the rainfall–aerosol interaction in central Amazonia. (1) Sub-40 nm particles frequently occur as bursts during rainfall events, probably associated with a series of reactions and the reduction of the condensation sink. (2) These bursts appear to be local features, occurring mostly below 325 m. They are not clearly observed at 325 m, and the model simulations indicate the main process occurs within and near the canopy. (3) The major sub-40 nm particle bursts occur together with injections of O_3 into or just above the canopy. (4) The maximum concentration of both particles and O_3 occurs around 0–30 minutes after the peak in rainfall. Furthermore, during this period, NO_2 also reaches its highest concentration, whereas NO, isoprene and monoterpene concentrations decrease to their minimum levels. (5) The condensation sink decreases with the rainfall, reaching its minimum value 30 minutes after the rain rate is at its maximum and facilitating the formation of the nucleation particles. (6) Model simulations indicate that the peak of HOMs and LVOCs and the biogenic nucleation rate occur mainly below 24 m, 30 minutes after the maximum rain rate. Finally, a clear growth process was observed in the early mornings after nights with ozone-rich air, typically following rain-rich days.

Figure 6 illustrates the atmospheric processes in the Amazon that occur during rain events in the afternoon/evening. The evolution of trace gas concentrations from the time before the onset of rain until up to 2 hours after the maximum precipitation suggests that the particle burst is produced by the reduction of the condensation sink and reactions involving O_3, terpenes and NO_x. Sesquiterpenes are likely to be a major player in particle formation. The growth process

occurring after sunrise on days following high nighttime O_3 concentrations suggests that the growth of sub-40 nm organic particles to the Aitken mode is initiated by high nighttime O_3 concentrations, followed by photo-oxidation processes in the morning. The high concentrations of O_3 injected into the canopy during the evening and night stay trapped in the nocturnal boundary layer, favouring the oxidation of organic compounds[44]. As soon as the sun rises, the total and oxidized organic aerosol concentrations close to the canopy sharply increase, moving the particle size from the nucleation mode to the Aitken and accumulation mode.

The locally formed nucleation particles grow mainly during the morning for the Aitken modes and are quickly transported to the free troposphere by the development of the convective boundary layer[42]. In the Amazon rainforest, three atmospheric layers can be defined with respect to the population of ultrafine particles: the mixed layer, between the surface and 1,200 m; a transitional layer between 1.2 and 4 km, called the convective cloud layer, where the lowest concentration of ultrafine particles is found; and the layer above, where the maximum concentration is near the tropopause[23,25]. Above the mixed layer, at about 1,500 m, are the low-level jets of the Amazon[45]. When a new convective cloud forms, the air currents in these particle-rich layers converge on the convective cell, and the particle-rich air is transported in updraughts and contributes to the formation of raindrops. Deep convection does not occur everywhere simultaneously but only in a few areas. Therefore, the flux convergence receives air from all directions in the neighbouring areas and can easily feed the CCN into these small regions where deep convective clouds occur. A simple calculation can be made to highlight the importance of the NPF on the Amazonian Green Ocean clouds. From the results of ref. 46, we can derive the linear equation describing the cloud droplet concentration with height in Amazonas and integrate from the cloud base to the cloud top at 4,000 m (freezing level and average cloud top height of cumulus clouds). From this calculation, we can estimate the number of warm cloud droplets at 450,000 per cm^2. Considering the NPF and the boundary-layer height of 1,000 m (ref. 47), there are about 250,000 particles per cm^2 in the boundary layer. If we now consider that the cloud cover near Manaus varies between 76% and 42% (ref. 48), and if we apply a factor to correct for the fact that we do not have clouds everywhere, we get a very close figure. This shows that the NPF processes in the boundary layer produce enough CCN for the Green Ocean clouds. Many other mechanisms produce CCN in the Amazon region, mainly from anthropogenic sources. However, only this mechanism can provide the basic background of CCN for the cumulus clouds in the remote forest region of the Amazon.

Finally, to test the hypothesis and prove whether ozonolysis is the main process in the formation of new particles in the boundary layer, we propose for future work the use of a chamber experiment at the canopy level, controlling the ozone concentration. The chamber should have a particle size magnifier to measure particles from 1 to 2 nm and a mass spectrometer to measure HOM composition, such as nitrate chemical ionization–atmospheric pressure interface time of flight. With this configuration, it will be possible to characterize the influence of ozone on particle formation.

Understanding the feedback mechanism between rainfall, trace gas and aerosol concentrations is of utmost importance on a planet experiencing a rapidly changing climate. The nucleation of particles, which subsequently become CCN and enable cloud formation, is closely tied to previous rainfall events. While anthropogenic emissions from biomass burning and fossil fuels can produce CCN, only this specific mechanism can generate the CCN concentrations required to create the Green Ocean Amazon pattern characteristic of the wet season. This pattern is distinguished by cloud droplet concentrations as low as a few hundred droplets at cloud base[49], of the same order as the newly formed particles described in this study.

Online content

Any methods, additional references, Nature Portfolio reporting summaries, source data, extended data, supplementary information, acknowledgements, peer review information; details of author contributions and competing interests; and statements of data and code availability are available at https://doi.org/10.1038/s41561-024-01585-0.

References

1. Köhler, H. The nucleus in and the growth of hygroscopic droplets. *Trans. Faraday Soc.* **32**, 1152–1161 (1936).
2. Albrecht, B. A. Aerosols, cloud microphysics, and fractional cloudiness. *Science* **245**, 1227–1230 (1989).
3. Pöhlker, M. L. et al. Long-term observations of cloud condensation nuclei in the Amazon rain forest—part 1: aerosol size distribution, hygroscopicity, and new model parametrizations for CCN prediction. *Atmos. Chem. Phys.* **16**, 15709–15740 (2016).
4. Kulmala, M. et al. Formation and growth rates of ultrafine atmospheric particles: a review of observations. *J. Aerosol Sci.* **35**, 143–176 (2004).
5. Arias, P. et al. *Technical Summary*. In *Climate Change 2021: The Physical Science Basis* (eds Masson-Delmotte, P. et al.) 33–144 (Cambridge Univ. Press, 2021).
6. Kerminen, V.-M. et al. Atmospheric new particle formation and growth: review of field observations. *Environ. Res. Lett.* **13**, 103003 (2018).
7. Andreae, M. & Rosenfeld, D. Aerosol–cloud–precipitation interactions. Part 1. The nature and sources of cloud-active aerosols. *Earth Sci. Rev.* **89**, 13–41 (2008).
8. Seinfeld, J. H. & Pandis, S. N. *Atmospheric Chemistry and Physics* 3rd edn (Wiley-Blackwell, 2016).
9. Ehn, M. et al. A large source of low-volatility secondary organic aerosol. *Nature* **506**, 476–479 (2014).
10. Tröstl, J. et al. The role of low-volatility organic compounds in initial particle growth in the atmosphere. *Nature* **533**, 527–531 (2016).
11. Kirkby, J. et al. Ion-induced nucleation of pure biogenic particles. *Nature* **533**, 521–526 (2016).
12. Andreae, M. O., Andreae, T. W., Ditas, F. & Pöhlker, C. Frequent new particle formation at remote sites in the subboreal forest of north america. *Atmos. Chem. Phys.* **22**, 2487–2505 (2022).
13. Artaxo, P., Maenhaut, W., Storms, H. & Van Grieken, R. Aerosol characteristics and sources for the Amazon basin during the wet season. *J. Geophys. Res. Atmos.* **95**, 16971–16985 (1990).
14. Pöschl, U. et al. Rainforest aerosols as biogenic nuclei of clouds and precipitation in the Amazon. *Science* **329**, 1513–1516 (2010).
15. Pöhlker, C. et al. Biogenic potassium salt particles as seeds for secondary organic aerosol in the Amazon. *Science* **337**, 1075–1078 (2012).
16. Rizzo, L., Artaxo, P., Karl, T., Guenther, A. & Greenberg, J. Aerosol properties, in-canopy gradients, turbulent fluxes and VOC concentrations at a pristine forest site in Amazonia. *Atmos. Environ.* **44**, 503–511 (2010).
17. Wimmer, D. et al. Ground-based observation of clusters and nucleation-mode particles in the Amazon. *Atmos. Chem. Phys.* **18**, 13245–13264 (2018).
18. Franco, M. A. et al. Occurrence and growth of sub-50 nm aerosol particles in the Amazonian boundary layer. *Atmos. Chem. Phys.* **22**, 3469–3492 (2022).
19. Machado, L. A. T. et al. How weather events modify aerosol particle size distributions in the Amazon boundary layer. *Atmos. Chem. Phys.* **21**, 18065–18086 (2021).
20. Pöhlker, M. L. et al. Aitken mode particles as CCN in aerosol- and updraft-sensitive regimes of cloud droplet formation. *Atmos. Chem. Phys.* **21**, 11723–11740 (2021).

21. Khadir, T. et al. Sink, source or something in-between? Net effects of precipitation on aerosol particle populations. *Geophys. Res. Lett.* **50**, e2023GL104325 (2023).
22. Ekman, A. M. L. et al. Do organics contribute to small particle formation in the Amazonian upper troposphere? *Geophys. Res. Lett.* https://doi.org/10.1029/2008GL034970 (2008).
23. Krejci, R. et al. Evolution of aerosol properties over the rain forest in Surinam, South America, observed from aircraft during the LBA-CLAIRE 98 experiment. *J. Geophys. Res. Atmos.* https://doi.org/10.1029/2001JD001375 (2003).
24. Bardakov, R. et al. A novel framework to study trace gas transport in deep convective clouds. *J. Adv. Model. Earth Syst.* **12**, e2019MS001931 (2020).
25. Andreae, M. O. et al. Aerosol characteristics and particle production in the upper troposphere over the Amazon basin. *Atmos. Chem. Phys.* **18**, 921–961 (2018).
26. Wang, J. et al. Amazon boundary layer aerosol concentration sustained by vertical transport during rainfall. *Nature* **539**, 416–419 (2016).
27. Liu, Y. et al. Strong particle production and condensational growth in the upper troposphere sustained by biogenic VOCs from the canopy of the Amazon basin. *Atmos. Chem. Phys.* **23**, 251–272 (2023).
28. Williamson, C. J. et al. A large source of cloud condensation nuclei from new particle formation in the tropics. *Nature* **574**, 399–403 (2019).
29. Bardakov, R., Krejci, R., Riipinen, I. & Ekman, A. M. L. The role of convective up- and downdrafts in the transport of trace gases in the Amazon. *J. Geophys. Res. Atmos.* **127**, e2022JD037265 (2022).
30. Wang, X., Gordon, H., Grosvenor, D. P., Andreae, M. O. & Carslaw, K. S. Contribution of regional aerosol nucleation to low-level CCN in an Amazonian deep convective environment: results from a regionally nested global model. *Atmos. Chem. Phys.* **23**, 4431–4461 (2023).
31. Davidson, E. A. et al. The Amazon basin in transition. *Nature* **481**, 321–328 (2012).
32. Andreae, M. O. et al. The Amazon Tall Tower Observatory (ATTO): overview of pilot measurements on ecosystem ecology, meteorology, trace gases, and aerosols. *Atmos. Chem. Phys.* **15**, 10723–10776 (2015).
33. Kulmala, M. et al. Measurement of the nucleation of atmospheric aerosol particles. *Nat. Protoc.* **7**, 1651–1667 (2012).
34. Gerken, T. et al. Downward transport of ozone rich air and implications for atmospheric chemistry in the Amazon rainforest. *Atmos. Environ.* **124**, 64–76 (2016).
35. Sigler, J. M., Fuentes, J. D., Heitz, R. C., Garstang, M. & Fisch, G. Ozone dynamics and deposition processes at a deforested site in the Amazon basin. *Ambio* **31**, 21–27 (2002).
36. Guenther, A. B. et al. The Model of Emissions of Gases and Aerosols from Nature version 2.1 (megan2.1): an extended and updated framework for modeling biogenic emissions. *Geosci. Model Dev.* **5**, 1471–1492 (2012).
37. Yáñez Serrano, A. M. et al. Diel and seasonal changes of biogenic volatile organic compounds within and above an Amazonian rainforest. *Atmos. Chem. Phys.* **15**, 3359–3378 (2015).
38. Schade, G. W., Goldstein, A. H. & Lamanna, M. S. Are monoterpene emissions influenced by humidity? *Geophys. Res. Lett.* **26**, 2187–2190 (1999).
39. Rossabi, S., Choudoir, M., Helmig, D., Hueber, J. & Fierer, N. Volatile organic compound emissions from soil following wetting events. *J. Geophys. Res. Biogeosci.* **123**, 1988–2001 (2018).
40. Faiola, C. L. et al. SOA formation potential of emissions from soil and leaf litter. *Environ. Sci. Technol.* **48**, 938–946 (2014).
41. Bourtsoukidis, E. et al. Strong sesquiterpene emissions from Amazonian soils. *Nat. Commun.* **9**, 2226 (2018).
42. Henkes, A., Fisch, G., MacHado, L. A. & Chaboureau, J. P. Morning boundary layer conditions for shallow to deep convective cloud evolution during the dry season in the central Amazon. *Atmos. Chem. Phys.* **21**, 13207–13225 (2021).
43. Williams, J., de Reus, M., Krejci, R., Fischer, H. & Ström, J. Application of the variability–size relationship to atmospheric aerosol studies: estimating aerosol lifetimes and ages. *Atmos. Chem. Phys.* **2**, 133–145 (2002).
44. Crounse, J. D., Nielsen, L. B., Jørgensen, S., Kjaergaard, H. G. & Wennberg, P. O. Autoxidation of organic compounds in the atmosphere. *J. Phys. Chem. Lett.* **4**, 3513–3520 (2013).
45. Anselmo, E. M., Schumacher, C. & Machado, L. A. T. The Amazonian low-level jet and its connection to convective cloud propagation and evolution. *Mon. Weather Rev.* **148**, 4083–4099 (2020).
46. Cecchini, M. A. et al. Illustration of microphysical processes in Amazonian deep convective clouds in the gamma phase space: introduction and potential applications. *Atmos. Chem. Phys.* **17**, 14727–14746 (2017).
47. Dias-Junior, C. Q. et al. Intercomparison of planetary boundary layer heights using remote sensing retrievals and ERA5 reanalysis over central Amazonia. *Remote Sens.* **14**, 4561 (2022).
48. Machado, L. A. T., Laurent, H., Dessay, N. & Miranda, I. Seasonal and diurnal variability of convection over the Amazonia: a comparison of different vegetation types and large scale forcing. *Theor. Appl. Climatol.* **78**, 61–77 (2004).
49. Cecchini, M. A. et al. Impacts of the Manaus pollution plume on the microphysical properties of Amazonian warm-phase clouds in the wet season. *Atmos. Chem. Phys.* **16**, 7029–7041 (2016).

Luiz A. T. Machado[1,2] ✉, Gabriela R. Unfer[1,3], Sebastian Brill[1], Stefanie Hildmann[4], Christopher Pöhlker[1], Yafang Cheng[5], Jonathan Williams[6,17], Harder Hartwig[6], Meinrat O. Andreae[1,7,8], Paulo Artaxo[2], Joachim Curtius[9], Marco A. Franco[10], Micael A. Cecchini[10], Achim Edtbauer[6], Thorsten Hoffmann[4], Bruna Holanda[1], Théodore Khadir[11], Radovan Krejci[11], Leslie A. Kremper[1], Yunfan Liu[1,12], Bruno B. Meller[2], Mira L. Pöhlker[3,13], Carlos A. Quesada[14], Akima Ringsdorf[6], Ilona Riipinen[11], Susan Trumbore[15], Stefan Wolff[1,16], Jos Lelieveld[6,17] & Ulrich Pöschl[1]

[1]Multiphase Chemistry Department, Max Planck Institute for Chemistry, Mainz, Germany. [2]Institute of Physics, University of Sao Paulo, Sao Paulo, Brazil. [3]Leibniz Institute for Tropospheric Research, Leipzig, Germany. [4]Chemistry Department, Johannes Gutenberg University, Mainz, Germany. [5]Aerosol Chemistry Department, Max Planck Institute for Chemistry, Mainz, Germany. [6]Atmospheric Chemistry Department, Max Planck Institute for Chemistry, Mainz, Germany. [7]Department of Geology and Geophysics, King Saud University, Riyadh, Saudi Arabia. [8]Scripps Institution of Oceanography, University of California San Diego, La Jolla, CA, USA. [9]Goethe University Frankfurt am Main, Frankfurt am Main, Germany. [10]Institute of Astronomy, Geophysics and Atmospheric Sciences, University of Sao Paulo, Sao Paulo, Brazil. [11]Department of Environmental Science and Bolin Centre for Climate Research, Stockholm University, Stockholm, Sweden. [12]School of Atmospheric Science, Nanjing University, Nanjing, China. [13]Faculty of Physics and Earth Sciences, Leipzig Institute for Meteorology, Leipzig University, Leipzig, Germany. [14]Coordination of Environmental Dynamics, National Institute for Amazonian Research, Manaus, Brazil. [15]Department of Biogeochemical Processes, Max Planck Institute for Biogeochemistry, Jena, Germany. [16]Weather Forecasting Services, German Meteorological Service, Offenbach, Germany. [17]Present address: Climate and Atmosphere Research Center, The Cyprus Institute, Nicosia, Cyprus. ✉e-mail: l.machado@mpic.de

Methods

SMPS and data processing

ATTO is situated 120 m above sea level and 150 km northeast of Manaus. The ATTO and the co-located Campina site are nested in the heart of the central Amazon rainforest within the Uatumã Sustainable Development Reserve. This pristine site has remained largely untouched by deforestation and is characterized by an ecosystem known as a lowland evergreen rainforest. The canopy rises between 30 and 40 m, and the trace gas and aerosol instrumentation used here spans from ground level up to 325 m. The particle number–size distribution measurements were collected from two SMPSs (TSI), each comprising a differential mobility analyser and condensation particle counter. Both SMPS systems were operated in parallel at two different sampling heights at the ATTO site. One SMPS was sampling from the 60 m inlet of the triangular mast and the second from the 325 m inlet of the Tall Tower. The two SMPS instruments cover a particle size range from 10 to 400 nm, and the sizing accuracy was frequently checked using monodisperse polystyrene latex particles. Data were acquired and exported with Aerosol Instrument Manager software (versions 9 and 10; TSI). The original temporal resolution was 5 minutes and this was converted to 30 minutes to maintain the same time resolution as the other data. The data were adjusted to standard temperature (273 K) and pressure (1,013.25 hPa). The theoretical losses due to the long inlets at 60 and 325 m were corrected on the basis of a methodology using size-dependent correction factors[50]. For the SMPS measurements at 60 m and 325 m, the composites were computed with 236 rain events, using the particle size distribution from 2018 to 2020. The robotic lift is an automatic elevator platform installed at ATTO's southern corner on the Tall Tower that allows continuous measurements of vertical profiles between 8 and 318 m. Its regular configuration carries an SMPS (NanoScan SMPS, Model 3910, TSI) along with various other counting and sizing instruments. SMPS data were collected during May 2023 following a strategy of consistently acquiring profiles at a rate of two per hour, where each profile takes 15 minutes to cover the 310 m elevation range. The data were compiled by selecting the 0–80 m and 240–320 m layers and computing the sub-20, sub-40, and sub-60 nm concentrations. The data were resampled to 30 minute time steps, which include one upward and one downward measurement. The 30 minute concentrations at 0–80 m and 240–320 m were analysed as a function of the rainfall events following the same methodology used in the other composites. During this month, the rain gauges at 81 m and 32 m had some gaps. A new dataset was built by combining the measured data at 81 m and 325 m with those of NASA's (National Aeronautics and Space Administration's) IMERG (Integrated Multi-satellite Retrievals for Global Precipitation Measurement) to produce one continuous data point every 30 minutes.

Composites and data processing

Composites were based on the time of maximum rainfall events (intensity greater than 0.5 mm h^{-1}) to analyse the evolution of different gases and particles during rainfall events. Tests were performed using the rainfall events at the maximum, the beginning and the end of the event, and the results were conceptually similar, except for the lag time. Composite analyses are useful tools with which to formulate physical hypotheses on the associations between environmental variables that occur over time[51] and to determine the basic characteristics of a particular phenomenon. Each rainfall event was selected in a 10 hour window with rain rate > 0.5 mm h^{-1}, and the time was selected as the maximum rain rate in this window. This analysis involves collecting large numbers of standardized cases (the maximum rainfall cases in each event) and compositing them with all other variables as a collection. The computing composite median and statistical significance (95%) of the selected pattern, in this case, the gas and particle concentrations during rainfall events, are computed.

Condensation sink

The condensation sink was based on the particle number–size distribution, similarly to ref. 18. The condensation sink (CS) is described by[33,52]

$$\mathrm{CS} = 2\pi D \int_{D_{p,\min}}^{D_{p,\max}} D'_p \beta_m \left(D'_p\right) n(D'_p)\, \mathrm{d}\, D'_p = 2\pi D \sum_{D'_p} \beta_m \left(D'_{p,i}\right) D'_{p,i} N_i \,[s^{-1}] \quad (1)$$

where N_i represents the particle concentration at the diameter $D'_{p,i}$ of the i-th size bin, D is the diffusion coefficient of the precursor condensable vapour, and β_m is the transition-regime correction[53]. The condensation sink quantifies the ability of particles to remove condensable vapours from the atmosphere, incorporating them into the particle population and directly influencing the particle growth. This study considers $D = 0.117\ \mathrm{cm^{-2}\ s^{-1}}$, the value for sulfuric acid (H_2SO_4) to obtain CS[54], commonly used in the literature for comparisons with other studies. In this study, each PNSD returned a single condensation sink based on equation (1), with a starting diameter of 10 nm and a final diameter of 400 nm, as described in the 'SMPS and data processing' section.

Box model

A box model was used to calculate the HOM and LVOC concentrations and the pure organic nucleation rate. We assume a steady state between production and loss for both HOMs and LVOCs, and then the concentration of HOMs ([HOM]) and LVOCs ([LVOC]) can be estimated, respectively, from

$$[\mathrm{HOM}] = \frac{Y_{\mathrm{AP.O_3}-\mathrm{HOM}}\, k_{\mathrm{AP.O_3}}\, [\mathrm{AP}]\, [\mathrm{O_3}]}{\mathrm{CS_{HOM}}} \quad (2)$$

$$[\mathrm{LVOC}] = \frac{Y_{\mathrm{AP.O_3}-\mathrm{LVOC}}\, k_{\mathrm{AP.O_3}}\, [\mathrm{AP}]\, [\mathrm{O_3}] + Y_{\mathrm{ISO.O_3}-\mathrm{LVOC}}\, k_{\mathrm{ISO.O_3}}\, [\mathrm{ISO}]\, [\mathrm{O_3}]}{\mathrm{CS_{LVOC}}} \quad (3)$$

where $Y_{\mathrm{AP.O_3}-\mathrm{HOM}} = 2.9\%$ is the HOM yield from the α-pinene oxidation by ozone[11], and the LVOC yields from the ozonolysis of α-pinene ($Y_{\mathrm{AP.O_3}-\mathrm{LVOC}}$) and isoprene ($Y_{\mathrm{ISO.O_3}-\mathrm{LVOC}}$) are assumed to be 13% and 3%[55], respectively. $k_{\mathrm{AP.O_3}}$ and $k_{\mathrm{ISO.O_3}}$ are the reaction rate constants for the oxidation of α-pinene and isoprene by ozone, respectively, the values of which follow the International Union of Pure and Applied Chemistry[56]. The concentration of α-pinene, [AP], is approximated by that of monoterpenes. $\mathrm{CS_{HOM}}$ and $\mathrm{CS_{LVOC}}$ are the CSs of HOMs and LVOCs, respectively, and are substituted by the condensation sink of H_2SO_4 as an approximation here. The pure biogenic nucleation rate (J_{org}), contributed by neutral and ion-induced processes[11], is parameterized as a function of HOM and ion concentration[27]. Here the model assumes the ion concentration as 500 $\mathrm{cm^{-3}}$, typical for the near-ground condition in boreal forests[57]. In addition, a temperature dependence of J_{org} is applied[58].

O_3, NO and NO_2 data processing periods

The vertical profiles of NO_x (NO and NO_2) and O_3 were obtained from 2014 to 2020 with an Ecophysics CLD TR 780 and a 49i ozone analyser (Thermo Scientific 49i), respectively[32,59]. The CLD measurements are based on a gas-phase chemiluminescence technique that directly retrieves the mixing ratio of NO. The NO_2 is measured through the conversion of NO_2 to NO by a photolytic converter, based on blue light (Solid-state Photolytic NO_2 Converter (BLC); DMT). The detection limits for NO and NO_2 are 0.05 and 0.1 ppb, respectively. The zero-point noise limits the signal noise to less than 0.5% of the signal. The O_3 measurements are based on the ultraviolet-absorption technique, which provides detection limits of 0.5 ppb. To reduce the effects of varying water vapour concentrations, the O_3 set-up uses Nafion dryers. To ensure high-quality measurements, the instruments were calibrated from time to time with a dynamic gas calibrator (Thermo Environmental Model 146C). This device has four different modes that are useful for obtaining

(1) the detection limits (zero air calibration), (2) NO calibration (gas dilution mode), (3) NO_2 calibration (gas-phase titration mode) and (4) O_3 calibration (transfer standard mode). The data were collected at the Instant tower at eight different heights (0.05, 0.5, 4, 12, 24, 38, 53 and 79 m), where 0.05 m is just above the surface and 79 m is about 40 m above the canopy. These different levels provide a good vertical resolution of the gas concentration. The gases were sampled every 5 minutes, and the time step was rescaled to 30 minutes for each height, the same period as the other aerosol and gas parameters used in this study. The O_3, NO and NO_2 measurements were collected from 2018 to 2020. Owing to the complexity of the NO and NO_2 measurements, there were several periods for which data were missing, which affected the compositing with the rainfall data. For O_3, 336 rain events were computed, but for NO and NO_2, only 114 and 94 rain events, respectively, were used for the composite.

Isoprene and monoterpene data processing periods

Observations of isoprene (C_5H_8) and monoterpenes ($C_{10}H_{16}$) at ATTO were conducted using a proton transfer reaction time-of-flight mass spectrometer (PTR-TOF-MS; Ionicon Analytik). It was operated with H_{30}^+ as primary ions, a drift tube pressure of 3.5 hPa and E/N (ratio of the electric field to the number density) of 120 Td. Isoprene (m/z 69.069) and monoterpenes (m/z 137.132) are detected with an uncertainty of about 20%. Their detection limits are 40 and 21 ppt, respectively. Mixing ratios were calibrated using a VOC (volatile organic compound) gas standard (Apel-Riemer Environmental), which contains isoprene and α-pinene to represent the sum of monoterpenes. To obtain a vertical profile of VOC mixing ratios, sample inlets (9.5 mm OD insulated Teflon) from 80 m, 150 m and 320 m were connected to the PTR-TOF-MS, installed at the foot of the ATTO tower. The sampling height varies with a frequency of 5 minutes. Thus, air from each height is analysed for 5 minutes every 15 minutes. Each inlet line was flushed before the sampling occurred. The data cover the period from 2018 to 2019. The data were resampled to 30 minutes. The composite with rainfall events was computed using 90 rainfall events during the wet season.

Weather data processing and periods

This study used local air temperature (T), relative humidity (RH), precipitation (P), and wind and solar radiation measured at the ATTO site from May 2013 to December 2016. The variables T and RH were measured using a Thermohygrometer (CS215, Rotronic Measurement Solutions), rainfall was obtained by a rain gauge (TB4, Hydrological Services), the wind parameters were obtained through a two-dimensional sonic anemometer (WindSonic, Gill Instruments) and the solar radiation with a net radiometer (NR-LITE2, Kipp & Zonen). All the instruments operate at a height of about 80 m on the Instant tower[18,32]. Rainfall data for 2018 and 2020 were collected at the ATTO tower. The composites were computed using 236 rain events.

Micro-orifice uniform deposition impactors data and experiment

Aerosol sampling was done with a micro-orifice uniform deposit impactor sampler (MSP, Model 125-R) connected to an aerosol inlet at 60 m height to collect aerosol particles according to their aerodynamic diameter. Thirteen stages, equipped with baked quartz filters (Whatman, QM-A), enabled sampling of particles covering diameters between 10 nm and 10 µm at a constant flow of 10 l $minute^{-1}$. Blank filters were collected by the same procedures, but with a HEPA filter (PALL 12144, HEPA capsule filter) connected between the aerosol inlet and the inlet of the micro-orifice uniform deposit impactor. Sampling was performed in May 2022 for 5 days at both heights. The aerosol sample analysis was performed using filter samples extracted three times by adding 1.5 ml of a 9/1 mixture of methanol and water (Fisher Scientific, Optima grade). The samples were subsequently agitated for 30 minutes on a laboratory shaker. The combined liquid phases were evaporated by a stream of N_2 (0.5 l^{-1}) using a Turbovap LV (Biotage) to approximate 200 µl. The residue was then filled to 1 ml with a 1/1 (v/v) mixture of water and acetonitrile (Fisher Scientific, Optima grade). The extracts were sonicated for 10 minutes and filtered through a 0.2 µm PTFE syringe filter (Carl Roth, Rotilabo KC 94.1). We added 5 µl of a 3,500 ppb solution of Camphor-10-sulfonic acid (Sigma Aldrich, 98%) in a 1/1 (v/v) mixture of water and acetonitrile (Fisher Scientific, Optima grade) as internal standard to correct the volume uncertainty. Ten microlitres of each sample were analysed three times by ultra-high-performance liquid chromatography (ThermoFisher Scientific, UltiMate 3000) coupled to a high-resolution Orbitrap mass spectrometer (ThermoFisher Scientific, Q Exactive). A heated electrospray ionization (ESI) source was installed and operated in the negative ionization mode. The instrument was externally calibrated with a calibration solution (Fisher Scientific, Pierce) and a 2 mM sodium acetate aqueous solution, providing mass accuracy below 1 ppm. The analysis was performed in the m/z 50–750 range at a mass resolving power of 140,000 at m/z 200. The following ESI-MS parameters were used for the measurements: ESI capillary temperature 300 °C; spray voltage 3.2 kV; sheath gas flow 30; auxiliary gas glow 10; S-lens RF level 50%. The ultra-high-performance liquid chromatography system was operated with an Acquity UPLC CSH fluoro-phenyl column (100 × 2.1 mm, 1.7 µm) from Waters and the mobile phase A (water with 2% acetonitrile and 0.04% formic acid) and mobile phase B (acetonitrile with 2% water). The conditions for gradient elution were as follows: 0–11 minutes, 10% B; 11–12 minutes, linear increase to 99% B; 12–12.5 minutes, linear decrease to 10% B; 12.5–13 minutes, 10% B at a constant flow rate of 500 µl $minute^{-1}$. The column temperature was maintained at 30 °C. To ensure the identification of β-nocaryophyllonic acid and β-caryophyllinic acid, standard compounds were synthesized as described by ref. 60. Fourteen-point calibration curves were generated with concentrations of β-nocaryophyllonic acid and β-caryophyllinic acid ranging from 0.5 ng ml^{-1} to 500 ng ml^{-1}. All reported values were normalized by the internal standard and field blank corrections.

ACSM data periods

The non-refractory aerosol species' fine-mode aerosol chemical composition measurements were performed using two quadrupole ACSMs (described previously[61]). The instrument vaporizes the non-refractory fraction of aerosols at around 600 °C to the gas phase and ionizes the resulting vapours by an electron beam. This process disintegrates the molecules, whose fragments are observed at their specific mass-to-charge ratios (m/z). Thereafter, the signal of each fragment is used to reconstruct the mass concentration of each chemical aerosol species (organic, nitrate, sulfate, ammonium and chloride) using a fragmentation table[62], which contains the known fragmentation pattern of each aerosol species. In addition, some specific compounds are used to gain insight into the aerosol composition. In particular, a high signal from the fragment with m/z of 44 (Org44), related mainly to CO_2^+, which was decomposed from organic aerosols, is a proxy for highly oxygenated organic aerosol[63]. The samples were collected from December 2021 to March 2022 simultaneously at 60 and 325 m heights at the ATTO site. The time resolution was 30 minutes. The data for each instrument were corrected for their air beam, flow rate, and collection and ionization efficiency through ammonium nitrate and ammonium sulfate calibrations. Then the dataset was averaged to a common time basis and corrected for standard temperature and pressure (273 K and 1,013.25 hPa). The aerosol range of measurement is from 75 nm to 650 nm.

Data availability

The datasets presented here are available on GitHub (https://gitlab.gwdg.de/luiz.machado/newparticleformation.git).

Code availability

The scripts are available on GitHub (https://gitlab.gwdg.de/luiz.machado/newparticleformation.git).

References

50. Von Der Weiden, S. L., Drewnick, F. & Borrmann, S. Particle Loss Calculator—a new software tool for the assessment of the performance of aerosol inlet systems. *Atmos. Meas. Tech.* **2**, 479–494 (2009).
51. Boschat, G., Simmonds, I., Purich, A., Cowan, T. & Pezza, A. B. On the use of composite analyses to form physical hypotheses: an example from heat wave–SST associations. *Sci. Rep.* **6**, 29599 (2016).
52. Dal Maso, M. et al. Condensation and coagulation sinks and formation of nucleation mode particles in coastal and boreal forest boundary layers. *J. Geophys. Res. Atmos.* **107**, D19 (2002).
53. Fuchs, N. A. & Sutugin, A. G. in *Topics in Current Aerosol Research* (eds Hidy, G. M. &. Brock, J. R.) (Elsevier, 1971).
54. Gong, Y. et al. Analysis on concentration and source rate of precursor vapors participating in particle formation and growth at Xinken in the Pearl River delta of China. *Adv. Atmos. Sci.* **25**, 427–436 (2008).
55. Gordon, H. et al. Reduced anthropogenic aerosol radiative forcing caused by biogenic new particle formation. *Proc. Natl Acad. Sci. USA* **113**, 12053–12058 (2016).
56. Atkinson, R. et al. Evaluated kinetic and photochemical data for atmospheric chemistry: volume II; gas-phase reactions of organic species. *Atmos. Chem. Phys.* **6**, 3625–4055 (2006).
57. Hõrrak, U. et al. Variation and balance of positive air ion concentrations in a boreal forest. *Atmos. Chem. Phys.* **8**, 655–675 (2008).
58. Dunne, E. M. et al. Global atmospheric particle formation from CERN CLOUD measurements. *Science* **354**, 1119–1124 (2016).
59. Nascimento, J. P. et al. Major regional-scale production of O_3 and secondary organic aerosol in remote Amazon regions from the dynamics and photochemistry of urban and forest emissions. *Environ. Sci. Technol.* **56**, 9924–9935 (2022).
60. van Eijck, A., Opatz, T., Taraborrelli, D., Sander, R. & Hoffmann, T. New tracer compounds for secondary organic aerosol formation from β-caryophyllene oxidation. *Atmos. Environ.* **80**, 122–130 (2013).
61. Ng, N. L. et al. An aerosol chemical speciation monitor (ACSM) for routine monitoring of the composition and mass concentrations of ambient aerosol. *Aerosol Sci. Technol.* **45**, 780–794 (2011).
62. Allan, J. D. et al. A generalised method for the extraction of chemically resolved mass spectra from aerodyne aerosol mass spectrometer data. *J. Aerosol Sci.* **35**, 909–922 (2004).
63. Canagaratna, M. R. et al. Elemental ratio measurements of organic compounds using aerosol mass spectrometry: characterization, improved calibration, and implications. *Atmos. Chem. Phys.* **15**, 253–272 (2015).

Acknowledgements

We thank all the people involved in the technical, logistical and scientific support of the ATTO project, particularly R. de Souza, B. Takeshi, R. Ditz, H. B. Xavier, A. R. Perreira, A. L. Matos, V. Ferreira de Lima, F. Alcinei, I. Diógenes, A. H. Melo do Nascimento and N. A. de Castro Souza. In addition, we thank J. Dominic for preparing a cartoon showing the processes involved in the formation of new particles. This research has been funded by the Bundesministerium für Bildung und Forschung (BMBF contracts 01LB1001A, 01LK1602B and 01LK2101B), the Brazilian Ministério da Ciência, Tecnologia e Inovação (MCTI/FINEP contract 01.11.01248.00), the Max Planck Society, the Conselho Nacional de Desenvolvimento Científico e Tecnológico (CNPq, Brazil) (process 200723/2015-4 and 407752/2023-4), the FAPESP (Fundação de Amparo à Pesquisa do Estado de São Paulo) (grant no. 2017/17047-0 and 2022/07974-0), the CNPq project (grant no. 169842/2017-7) and the CAPES project (grant no. 88887.368025/2019-00). For the operation of the ATTO site, we acknowledge the support by the Instituto Nacional de Pesquisas da Amazônia (INPA), the Amazon State University (UEA), the Large-Scale Biosphere–Atmosphere Experiment (LBA), FAPEAM, the Reserva de Desenvolvimento Sustentável do Uatumã (SDS/CEUC/RDS-Uatumã) and the Max Planck Society. This paper contains results of research conducted under the Technical/Scientific Cooperation Agreement between the National Institute for Amazonian Research, the State University of Amazonas, and the Max-Planck-Gesellschaft e.V.; the opinions expressed are the entire responsibility of the authors and not of the participating institutions.

Author contributions

CDL.A.T.M., C.P., J.W. and H.H. conceived and designed the study. L.A.T.M., M.A.C., G.R.U., M.A.F., A.R., L.A.K., B.B.M., S.B., S.H., M.L.P., A.R., B.H., J.C., M.A.C., A.E., T.K., R.K., I.R. and S.W. worked on data curation and interpretation. U.P., P.A., J.L., T.H., C.A.Q., C.P. and S.T. were responsible for funding acquisition and management. L.A.T.M. developed the methodology and carried out the data analysis. Y.C. and Y.L. ran and analysed the box model; L.A.T.M., C.P., U.P. and M.O.A. wrote the original draft, with all authors contributing to and revising the text.

Funding

Open access funding provided by Max Planck Society.

Competing interests

The authors declare no competing interests.

Additional information

Supplementary information The online version contains supplementary material available at https://doi.org/10.1038/s41561-024-01585-0.

Correspondence and requests for materials should be addressed to Luiz A. T. Machado.

Peer review information *Nature Geoscience* thanks the anonymous reviewer(s) for their contribution to the peer review of this work. Primary Handling Editor: Xujia Jiang, in collaboration with the *Nature Geoscience* team.